Separation Science and Technology
Publication details, including instructions for authors and subscription information:
http://www.informaworld.com/smpp/title~content=t713708471

Equilibrium Behavior in Acid-Base Chromatography for Carbon Isotope Separation

Kunihiko Takeda[a]; Heiichiro Obanawa[a]; Naoki Morita[a]
[a] URANIUM ENRICHMENT RESEARCH LABORATORY (KAWASAKI) ASAHI CHEMICAL INDUSTRY CO., LTD., KAWASAKI, JAPAN

To cite this Article Takeda, Kunihiko , Obanawa, Heiichiro and Morita, Naoki(1987) 'Equilibrium Behavior in Acid-Base Chromatography for Carbon Isotope Separation', Separation Science and Technology, 22: 1, 103 — 119
To link to this Article: DOI: 10.1080/01496398708056161
URL: http://dx.doi.org/10.1080/01496398708056161

SEPARATION SCIENCE AND TECHNOLOGY, **22**(1), pp. 103-119, 1987

Equilibrium Behavior in Acid-Base Chromatography for Carbon Isotope Separation

KUNIHIKO TAKEDA,* HEIICHIRO OBANAWA, and NAOKI MORITA

URANIUM ENRICHMENT RESEARCH LABORATORY (KAWASAKI)
ASAHI CHEMICAL INDUSTRY CO., LTD.
1-3-2, YAKO, KAWASAKI-KU, KAWASAKI 210, JAPAN

Abstract

The separation of ^{12}C and ^{13}C isotopes by acid-base chromatography using an anion-exchange resin was investigated. In order to design the separation system, equilibria with respect to a carbon band were examined with reduction potential strength. Simulation and analysis with the potential strength and the newly derived S and L potentials were found useful for determining experimental conditions. Isotopic separation factors between CO_2 and HCO_3^- observed in the chromatographic experiments were nearly equal to those in the corresponding solutions. The experiments at 25 or 90°C gave values of about 1.25 to 1.26×10^{-2} as the isotropic molar ratio of ^{13}C at the rear boundary of the carbon band.

INTRODUCTION

Isotope separation of carbon, nitrogen, and oxygen elements has been actively studied (*1*). Several chemical exchange reactions have been investigated for recovering ^{13}C. An equilibrium between HCN(gas) and NaCN(solution) is an effective reaction with the isotopic separation factor reported to be comparatively large, 0.012 (*2*). It could be applied to separation methods such as distillation and chemical exchange (*3*).

The isotope equilibrium of CO_2/HCO_3^- in Eq. (1) was also studied by

*To whom correspondence should be addressed.

Urey (*4*) and Reid (*5*) who reported the isotopic separation factor to be 0.007–0.016:

$$H^{12}CO_3^- + {}^{13}CO_2 \rightleftharpoons H^{13}CO_3^- + {}^{12}CO_2 \quad (1)$$

This reaction is suitable for a practical separation process because the chemical species involved are nontoxic. We applied our methods of analyzing chemical equilibria and separating uranium isotopes (*6–8*) to carbon isotope separation. In this study, chemical equilibria were analyzed through reduction potential strength and newly derived S and L potentials, and acid-base chromatography was designed by analogy of the redox chromatography for uranium isotope separation.

PRELIMINARY CONSIDERATIONS

Isotope separation using an ion-exchange resin can be accomplished by elution chromatography, where a solution containing the sorbable materials is fed to the top of an ion-exchange column, and then the materials are eluted by a developing agent. Generally speaking, elution chromatography is a simple and convenient procedure, but it is not always a superior method for isotope separation. Displacement chromatography, where the materials to be separated are inhibited from diffusing through both boundaries of an adsorption zone, is an excellent method for separating isotopes, including carbon isotopes. The reason is as follows: Even under the condition of a large development distance, which is essential for isotope separation due to the small separation factor, displacement chromatography keeps material concentrations high, while in elution chromatography the material concentrations are greatly decreased, resulting in an impractical dilution of the material.

Two agents which react with carbonic species at both boundaries are necessary for displacement chromatography, and an acid and an alkali were selected as those reactive agents. As for the two chemical species in Eq. (1), HCO_3^- is adsorbed on the anion-exchange resin and CO_2 is dissolved in the solution under pressure. The solubility of CO_2 in an aqueous solution is 0.033 mol/dm^3 at $P = 9.80 \times 10^4$ Pa and 0.33 mol/dm^3 at $P = 9.80 \times 10^5$ Pa. The acid dissociation constants are $pK_{a1} = 6.4$ for HCO_3^-/CO_2 and $pK_{a2} = 10.5$ for CO_3^{2-}/HCO_3^- at 298 K. The pH dependence of distribution of the carbonic species in an aqueous solution is shown in Fig. 1, where the dashed lines show the proportions of dissociated forms of a weakly anionic exchange resin (A) with a pK_a of 5.6 and a strongly anionic exchange resin (B). Since HCO_3^- must coexist with

carbon dioxide in solution in order to form a bicarbonate adsorption band, a pH range from 4 to 5 seems preferable, judging from the distribution curves in Fig. 1.

EXPERIMENTAL

Carbon dioxide gas was 99.5% pure and contained H_2O, N_2, and CH_4 as impurities. NaOH and HCl were obtained from Merck Co. The starting polymer, which was subsequently transformed to the ion-exchange resin, was prepared by polymerizing 83 parts of chloromethylstyrene with 17 parts of *m*-divinylbenzene. The polymer was reacted with diethylamine to give a weakly basic anion-exchange resin and with triethylamine to give a strongly basic anion-exchange resin. The ion-exchange resin thus prepared was packed in a stainless steel column that was 10 mm in diameter and 1000 mm in length. 0.1 mol/dm^3 aqueous NaOH and an aqueous solution of CO_2 at 9.80×10^5 Pa were fed successively into the column at the top. The adsorption band of HCO_3^- was developed by 0.1

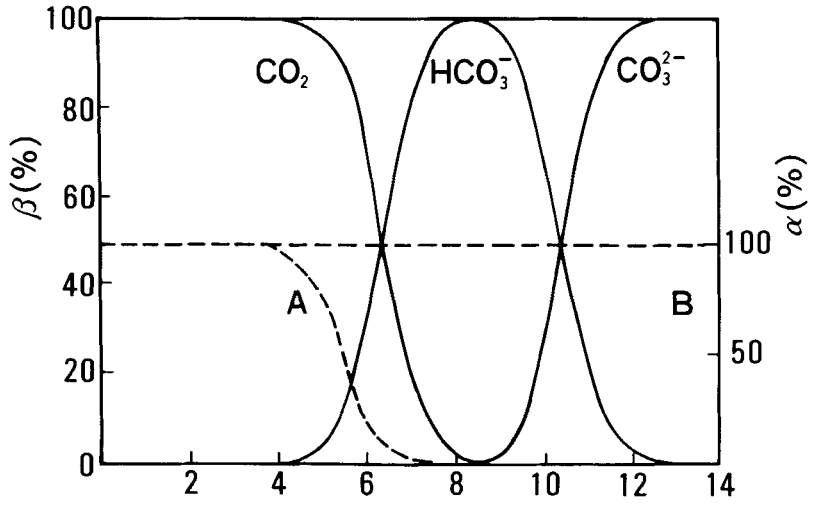

FIG. 1. Distributions of carbonate, bicarbonate, and carbon dioxide, and anion-exchange resin as a function of pH. β = distribution ratio of carbonic species (%), α = ratio of dissociated form of ion-exchange resin (%), A = weakly anionic exchange resin, B = strongly anionic exchange resin.

mol/dm^3 HCl. The temperature and the pressure of operation were changed as necessary. The eluant was recovered from the bottom of the column and fractionated into several tens of portions under pressure. The samples were analyzed by a mass spectrometer to measure the isotopic ratio.

Some devices and cautions in operating the instrument were required to measure isotopic ratios accurately.

(a) It was essential to avoid the intrusion of moisture into the ion source. Otherwise some chemical species, which had the same mass number as $^{12}CO_2^+$ or $^{13}CO^{2+}$, were introduced or generated there. The peaks of mass numbers 44 and 45 apparently tended to increase with increasing water content.
(b) The flow rate of a gasified sample introduced into the ion source should be kept constant. Otherwise, separation of $^{13}CO_2$ and $^{12}CO_2$, which occurs at the nozzle located in the upstream part of the ion source, was not efficient.

A double trap for freezing water and carbon dioxide separately was connected through the vacuum line with the ion-source inlet for the first requirement (a), and a specially devised gas inlet line with both a carbon-dioxide reservoir and a precision needle valve was installed for the second requirement (b). The extent of experimental errors was checked. The isotopic ratios of the natural carbon dioxide samples were found to be $(1.177 \pm 0.005) \times 10^{-2}$ reproducibly.

BASIC PRINCIPLE OF ACID-BASE CHROMATOGRAPHY

Acid-base chromatography has a mechanism similar to redox chromatography whose basic principle was described in a previous paper (*9*). Protons force ions to be desorbed from the stationary phase in acid-base chromatography just as electrons do in redox chromatography. The procedure and the basic principle of acid-base chromatography are briefly described below.

Solutions containing 1) alkali, 2) dissolved carbon dioxide, and 3) acid are fed into a column successively. Three zones are formed in the column as shown in Fig. 2: the alkaline zone, the carbon zone, and the acid zone. At the front boundary of the carbon zone, CO_2 flowing down in the mobile phase reacts with a hydroxide ion on the anion-exchange resin and is changed to HCO_3^- which stays in the stationary phase. At the rear boundary the HCO_3^- loaded on the resin reacts with the acid and is

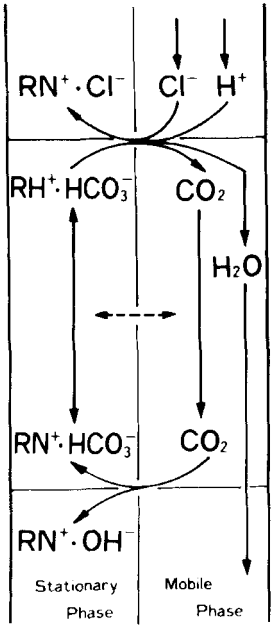

Rear boundary

$$RN^+ \cdot HCO_3^- + HCl \longrightarrow RN^+ \cdot Cl^- + CO_2 + H_2O$$

Carbon zone

$$H^{12}CO_3^- + {}^{13}CO_2 \longrightarrow H^{13}CO_3^- + {}^{12}CO_2$$

(isotopic exchange reaction)

Front boundary

$$RN^+ \cdot OH^- + CO_2 \longrightarrow RN^+ \cdot HCO_3^-$$

FIG. 2. Basic composition and principle of acid-base chromatography for carbon isotope separation.

transformed to CO_2 which flows downward in the mobile phase. In the bicarbonate adsorption zone (termed "carbon zone" in Fig. 2), the isotope-exchange reaction (as shown in Eq. 1) occurs in the mobile phase in each imaginary equilibrium stage. As the carbon zone is forced down by acid fed at the top of the column, the reactions at both boundaries are repeated.

The principle of separation in acid-base chromatography is similar to that of distillation because the reactions at both boundaries can be regarded as reflux and reboil. Carbon-13 isotope, which corresponds to a lighter component in distillation, accumulates at the rear boundary, while carbon-12 isotope, corresponding to a heavier component, accumulates at the front boundary.

BASIC EQUILIBRIA OF ACID-BASE CHROMATOGRAPHY

The individual reactions of the carbonic species occurring in this type of chromatography can be expressed as follows. (a) Acid-base reactions:

$$CO_2 + OH^- \rightleftharpoons HCO_3^- \quad (2)$$

$$HCO_3^- + OH^- \rightleftharpoons CO_3^{2-} + H_2O \quad (3)$$

(b) Ion-exchange reactions:

$$OH^- + RN^+ \rightleftharpoons RN^+ \cdot OH^- \quad (4)$$

$$HCO_3^- + RN^+ \rightleftharpoons RN^+ \cdot HCO_3^- \quad (5)$$

$$CO_3^{2-} + 2RN^+ \rightleftharpoons (RN^+)_2 \cdot CO_3^{2-} \quad (6)$$

$$Cl^- + RN^+ \rightleftharpoons RN^+ \cdot Cl^- \quad (7)$$

where RN^+ is a fixed ionic group on the anion-exchange resin. At the front boundary, Reactions (2), (4), and (5) occur simultaneously, and the overall exchange reaction is

$$RN^+ \cdot OH^- + CO_2 \rightleftharpoons RN^+ \cdot HCO_3^- \quad (8)$$

At the rear boundary, Reactions (2), (5), and (7) occur concurrently, and the overall exchange reaction can be written

$$RN^+ \cdot HCO_3^- + H^+ + Cl^- \rightleftharpoons RN^+ \cdot Cl^- + CO_2 + H_2O \quad (9)$$

At both boundaries as well as in the bicarbonate adsorption band, Reactions (3) and (6) are negligible since a carbonate ion cannot exist at pH = 7 or less as shown in Fig. 1.

In the bicarbonate adsorption band, the carbon-carbon isotopic exchange reaction occurs stepwise: the first step is a proton-exchange reaction between a bicarbonate ion and carbon dioxide dissolved in the solution, where the isotope effect is probable; the second step is the ion-exchange reaction shown in Eq. (5), where an appreciable isotope effect is not observed.

Equations (2)–(7) can be uniformly expressed in addition form as

$$A + \nu X \rightleftharpoons D \quad (10)$$

where A is CO_2, HCO_3^-, or CO_3^{2-} (an acceptor); X is OH^-, H^+, or RN^+ (an addend); D is any species on the right-hand side of Eqs. (2)–(7) (an adduct); and ν is the stoichiometric coefficient of the addend, X.

Since the standard reduction potential strength $\Delta\mu^\circ_{A/D}$ and the potential strength $\Delta\mu_X$ are defined as

$$\Delta\mu^{\circ}_{A/D} \equiv \mu^{\circ}_{X} - \frac{\mu^{\circ}_{D} - \mu^{\circ}_{A}}{\nu} \tag{11}$$

and

$$\Delta\mu_{X} \equiv \mu^{\circ}_{X} - \mu_{X} \tag{12}$$

the equilibrium relationship of Eq. (10) is expressed quantitatively as

$$\Delta\mu_{X} = \Delta\mu^{\circ}_{A/D} + \frac{RT}{\nu} \ln \frac{\alpha_{A}}{\alpha_{D}} \tag{13}$$

QUANTITATIVE CONSIDERATION OF ACID-BASE CHROMATOGRAPHY

The molar ratio of an arbitrary adduct D that is a mixed-addend complex of a given *i*th species of A with n_j units of an arbitrary *j*th species of X, to the "naked" *i*th species of A, can be expressed as

$$T_{i,n_j} = \exp \frac{S_p - L_p}{RT} \tag{14}$$

where

$$S_p = \sum_{j} \sum_{n_j} \nu_{i,n_j} \cdot \Delta\mu^{\circ}_{i,n_j} \tag{15}$$

and

$$L_p = \sum_{j} \sum_{n_j} \nu_{i,n_j} \cdot \Delta\mu_{i,n_j} \tag{16}$$

The distribution function given by Eq. (14) is seemingly complicated, and this new theoretical derivation is regarded as a trivial or overcomplicated attempt. However, the numerical solution can be easily obtained because the function is always of a monotonous increase and leads to only one solution, which is important for computer simulation of chromatography. The conventional methods, where functions containing equilibrium constants K are used, are not suitable for practical use since several roots are obtained, making it hard to select a true solution. Because a procedure for reaching the solution must be repeated for each

imaginary equilibrium stage in chromatography, its efficiency results in a great difference in the quantity of work needed.

The S_p (S potential) is specific to each adduct species formed and thus constant, since it is the sum of standard reduction potential strengths, $\Delta\mu_i^\circ$, of stepwise addition reactions of individual addends to a given acceptor, as is evident from Eq. (15). The L_p (L potential) is characteristic of the state of a solution that is determined by the activity of each addend species in the solution. Semiquantitative consideration can be made with S_p and L_p, and a more detailed simulation of chromatography is made from computer calculations with the distribution function T_{i,n_j} for imaginary equilibrium stages in a chromatography column.

The standard reduction potential strengths are shown in Table 1, where the potential strengths in Reactions (17) to (20) are calculated using published data (*10*), and those in Reactions (21) to (24) were measured in this study. The potential strength for Cl^- ion exchange is set at 0 kJ/mol since it is chosen as the standard ion for ion-exchange reactions. Figure 3 shows the systematic diagram of the $\Delta\mu^\circ$ of the carbonic species, where CO_2 is the "naked" acceptor species and OH^- and RN^+ are addends. The S potentials, which were calculated from this diagram, are shown in Table 2. The second column of Table 2 shows the abbreviated notation of the chemical species, where the first number in parentheses is the addition numbers of OH^- and the second the numbers of RN^+. In Fig. 3 and Table 2, $CO_2 \cdot (OH^-)$, $CO_2 \cdot (OH^-)_2$, $CO_2 \cdot (OH^-)(RN^+)$, and $CO_2 \cdot (OH^-)_2(RN^+)_2$ denote HCO_3^-, CO_3^{2-}, $RN^+ \cdot HCO_3^-$, and $(2RN^+) \cdot CO_3^{2-}$, respectively. Generally speaking, the addition of OH^- (acid-base

TABLE 1
Standard Reduction Potential Strength of Various Reactions in a CO_2-Containing Chromatography System

	Reaction	$\Delta\mu^\circ$ (kJ/mol)
(17)	$CO_2 + OH^- \rightarrow HCO_3^-$	$\Delta\mu_1^\circ$: 43.64
(18)	$HCO_3^- + OH^- \rightarrow CO_3^{2-} + H_2O$	$\Delta\mu_2^\circ$: 20.92
(19)	$Na^+ + OH^- \rightarrow NaOH$	$\Delta\mu_3^\circ$: −39.96
(20)	$H^+ + Cl^- \rightarrow HCl$	$\Delta\mu_4^\circ$: −39.96
(21)	$OH^- + RN^+ \rightarrow RN^+ \cdot OH^-$	$\Delta\mu_5^\circ$: −5.98
(22)	$Cl^- + RN^+ \rightarrow RN^+ \cdot Cl^-$	$\Delta\mu_6^\circ$: 0.00
(23)	$HCO_3^- + RN^+ \rightarrow RN^+ \cdot HCO_3^-$	$\Delta\mu_7^\circ$: −2.79
(24)	$CO_3^{2-} + 2RN^+ \rightarrow (2RN^+) \cdot CO_3^{2-}$	$\Delta\mu_8^\circ$: −15.23

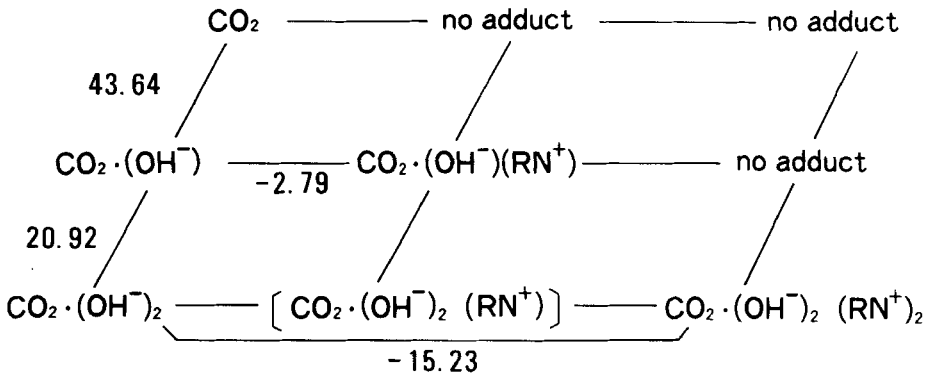

FIG. 3. Systematic diagram of standard reduction potential strengths ($\Delta\mu°$, kJ/mol) of carbonic species.

reaction) and ion exchange cannot be treated on a common scale, and the equilibrium constants of both reactions are defined by different notations with different dimensions. Both of these reactions, however, can be treated with the same equilibrium factor ($\Delta\mu°$), and the stabilization energy of each species can be directly represented by S_p.

The results of chromatography simulation using the values of S_p listed in Table 2 are shown in Fig. 4. The scale on the horizontal axis denotes the order of a successive equilibrium state determined along the imaginary flow, and the vertical axis represents potentials S_p and L_p. Here, it should be remembered that the potential difference, $S_p - L_p$, of a given adduct is the scale of its stability, as shown in Eq. (14). In the notation $L_p(1,0)$, the first number in parentheses refers to the addition number of OH^- to carbon dioxide in solution and the second that of RN^+, as in the notation of the chemical species for S_p in Table 2. Thus, $L_p(1,0)$ refers to the L_p of a bicarbonate ion.

The simulation shown in Fig. 4 started with imaginary feeding of a carbon dioxide solution to the top of the column which is packed with an anion-exchange resin regenerated in advance by an alkaline solution.

In the steps from the 380th to the 500th, CO_2 is considered to be the main carbonic species in the mobile phase since $S_p(1,0) < L_p(1,0)$ and $S_p(2,0) < L_p(2,0)$, while HCO_3^- is considered to be predominant in the stationary phase from the relations $S_p(1,1) > L_p(1,1)$, $S_p(2,2) < L_p(2,2)$, and most probably $S_p(0,1) \ll L_p(0,1)$.

In the steps up to the 370th, HCO_3^- could be the main mobile-phase

TABLE 2
S Potentials of Carbonated Chemical Species in the Case Where CO_2 Is a Standard Chemical Species

Chemical species		S potential (kJ/mol)
CO_2	$CO_2(0,0)$	0
$CO_2 \cdot (OH^-)$	$CO_2(1,0)$	43.64
$CO_2 \cdot (OH^-)_2$	$CO_2(2,0)$	64.56
$CO_2 \cdot (OH^-)(RN^+)$	$CO_2(1,1)$	40.84
$CO_2 \cdot (OH^-)_2(RN^+)$	$CO_2(2,1)$	—
$CO_2 \cdot (OH^-)_2(RN^+)_2$	$CO_2(2,2)$	34.10

species since the $S_p(1,0) \approx L_p(1,0)$ relation is reversed to $S_p(1,0) > L_p(1,0)$, which means descending CO_2 may be transformed to HCO_3^-. However, most HCO_3^- ions in the mobile phase will not stay there but migrate into the stationary phase, from the relation $S_p(1,1) \gg L_p(1,1)$, resulting in the formation of the front boundary.

Passing the 500th step, the stationary-phase bicarbonate ions will disappear because the potential difference, $S_p(1,1) - L_p(1,1)$, turns negative, and carbon dioxide also disappears rapidly from the mobile phase. This rapid disappearance of all carbonic species ensures the formation of the rear boundary around the 500th step. It can be understood that after the 500th step, bicarbonate ions on the resin are desorbed, undergoing simultaneous transformation to carbon dioxide which then flows downward.

RESULTS AND DISCUSSION

Based on the theoretical considerations and a number of computer simulations, several experiments were conducted under different conditions. The variable parameters were 1) the concentrations of base, acid, and carbon dioxide in solution; 2) the basicity of the anion-exchange resin; 3) temperature and pressure, and 4) column length. Table 3 shows the experimental conditions and Table 4 shows the experimental results. Plots of total carbon concentration and isotopic molar ratio vs elution volume, measured in Experiment 4, are shown in Fig. 5. Dissolved CO_2 appeared in the fraction at 0.11 dm^3 of elution volume, and a plot of the total carbon concentration vs elution volume formed a trapezoidal shape which is characteristic of displacement chromatography. The isotopic ratio of ^{13}C was the lowest when a CO_2-containing solution began to flow

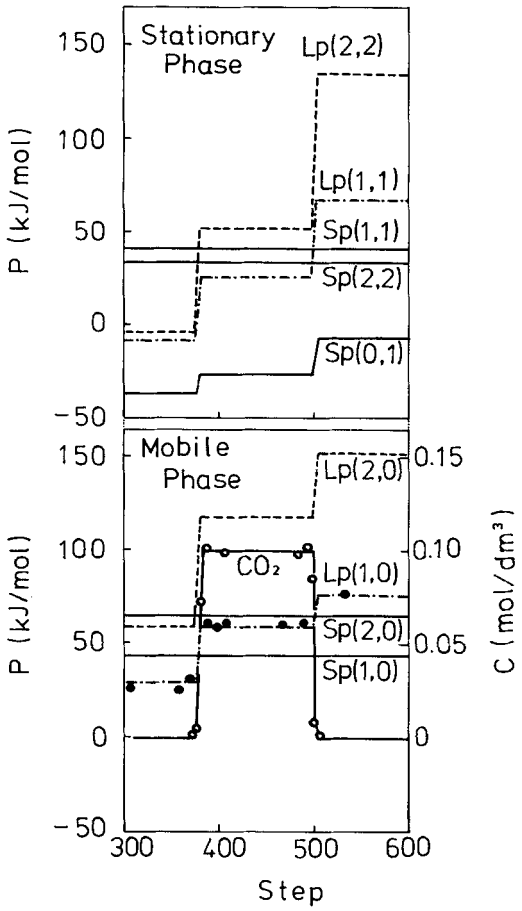

FIG. 4. Potentials (L_p and S_p) from computer simulations and concentration of dissolved CO_2 (C). (●) $L_p(1,0)$ observed, (○) measured concentration of dissolved CO_2.

out and increased with increasing elution volume. The ratio of ^{13}C recorded the highest value of 1.248×10^{-2} at the moment the total carbon concentration of effluent was reduced drastically. The degree of separation was found to be 5.4% while the isotopic separation factor of ^{13}C was observed to be 0.012. The corresponding plots for all the other experiments also formed a trapezoid with steep hillsides. The experimental results thus obtained are considered to support the predictive analysis of the separation mechanism based on the equilibrium consideration and the computer simulations.

TABLE 3
Experimental Conditions of Acid-Base Chromatography

Experiment	Type of ion-exchange resin	Temperature (°C)	Concentration (mol/dm^3)	
			NaOH	HCl
1	Strongly basic	25	0.1	0.1
2	Strongly basic	25	0.01	0.01
3	Weekly basic	25	0.1	0.1
4	Weekly basic	25	0.01	0.01
5	Weekly basic	90	0.1	0.1
6	Weekly basic	90	0.01	0.01

Similar results were obtained in the other experiments, as shown with Experiment 4 in Table 4. The observed isotopic separation factors were within a narrow range from 0.009 to 0.013. This indicates that the isotope exchange reactions in the imaginary equilibrium stages seem to have been stable due to the constancy of the total carbon concentration. The degree of separation was also in a narrow range of 5 to 6% at both front and rear boundaries. The acid-base displacement chromatography is excellently stable during operation because the reactions at both boundaries are very fast and the changes of the two potentials (L_p and S_p) are very discrete at both boundaries.

TABLE 4
Results of the Separation of Carbon Isotopes

Experiment	Isotopic molar ratio (X 10^{-2})		Separation factor
	Front	Rear	
1	1.119	1.245	0.012
2	1.117	1.247	0.013
3	1.113	1.250	0.012
4	1.113	1.248	0.012
5	1.098	1.259	0.009
6	1.099	1.258	0.009

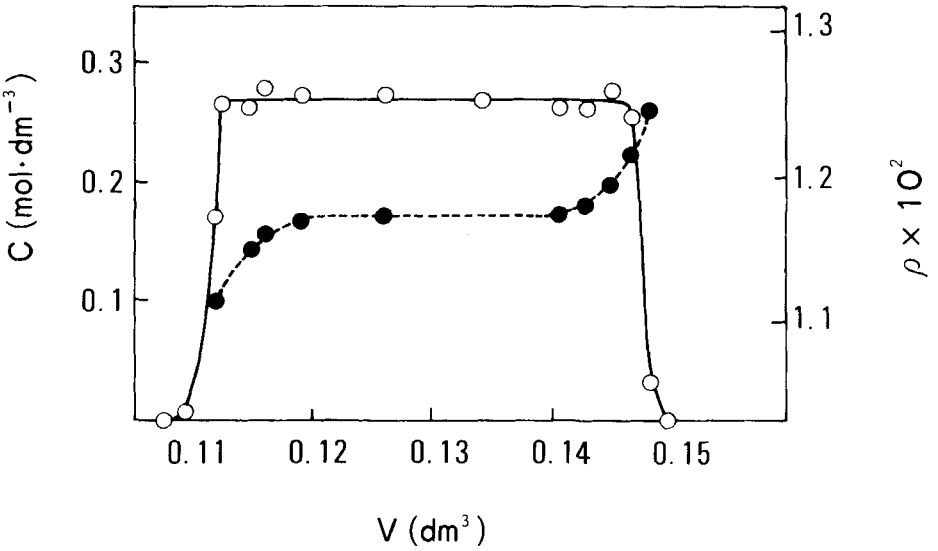

FIG. 5. Plots of total carbon concentration (C) and isotopic molar ratio of $^{13}C(p)$ vs elution volume in Experiment 4. (O) Total carbon concentration, (●) isotopic molar ratio, V = elution volume.

PRELIMINARY CONSIDERATIONS OF CHROMATOGRAPHIC KINETICS

If we denote with C the concentration of each isotope species and with Z the vertical axis of the column, the microscopic movement can be accurately expressed by the following equation (*11*):

$$\frac{\partial C}{\partial t} = -v\frac{\partial C}{\partial Z} + D\frac{\partial^2 C}{\partial Z^2} \tag{25}$$

where v and D are the mean migration velocity of band and the effective diffusion coefficient, respectively.

In the present case, where a reversible chemical reaction takes place between a bicarbonate ion and a molecule of carbon dioxide, the plate height H depends on the rate constants of chemical change of the carbonic species in both the mobile and stationary phases as well as those of the adsorption-desorption processes. The plate height here refers to the height of a compartment small enough to allow an isotopic

equilibrium between the stationary-phase species and the mobile-phase species, as given by Eq. (1). The latter species eventually leaves the compartment as soon as equilibrium is attained. The kinetic picture of all these processes is shown in Fig. 6.

The plate height expression is normally complex, but in this case it reduces in the first approximation to a rather simple equation:

$$H = \frac{2(X_2 + X_3)(X_1 + X_4)v}{k_{12}} + \frac{2X_3(X_1 + X_4)^2 v}{k_{32}(X_2 + X_3)} + H_m \qquad (26)$$

where $k_{12} = 60D/dp^2$, where dp is the average resin diameter, D is the effective diffusion coefficient within a resin particle, and k_{32} is the ligand exchange rate constant, k_L. This simplification is justified because both k_{14} and k_{34} are much smaller than the other rate constants.

In our preliminary measurements, the effective diffusion coefficient (D) was about 1.5×10^{-6} cm^2/s at 25°C and 3.7×10^{-6} cm^2/s at 90°C, and its activation energy was 12.6 kJ/mol. The rate constant of ligand exchange (k_L) was found to be 6.0×10^{-2} s^{-1} at 25°C and 5.4 s^{-1} at 90°C, and its activation energy was 62.4 kJ/mol.

The third term on the right-hand side of Eq. (26), H_m, is very complicated, being composed of several separate terms such as a long-range interaction term and a short-range interaction term. In our experiments up to now, H_m was determined to be about 1200 μm, but

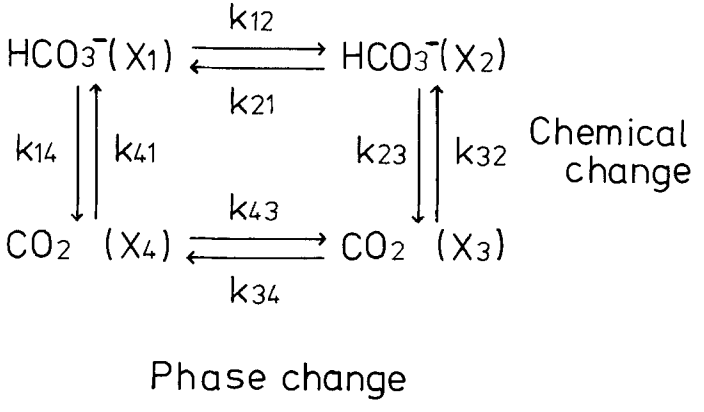

FIG. 6. Kinetic picture of equilibria between CO_2 and HCO_3^- in the presence of anion-exchange resin.

much remains to be done to analyze it more precisely. We are now studying the kinetics.

The first and second terms on the right-hand side of Eq. (26) can be estimated by taking advantage of these values of D and k_L together with the distribution constant of each chemical species between both phases.

INDUSTRIAL APPLICATION OF ^{13}C ISOTOPE SEPARATION

Figure 7 shows a flow diagram of the actual configuration in which the carbon band is developed continuously. The separation module in the center of the figure is composed of more than two columns with two selector values attached to each column, which together effectively form the circular path. The feed and recovery section of the carbonic solution is shown on the left of the separation module. One selector valve in the recirculation path of the carbon band is used for both feeding the natural carbon dioxide solution to the band and for recovering enriched and depleted ^{13}C from the band. The acid-base section is shown on the right of the module. The salt produced in the column is disposed of while fresh acid and base solutions necessary for continuous separation are fed. Electric power is required to pump the acid and base solutions into the separation module.

The economics of ^{13}C enrichment by the acid-base chromatography process still remain to be proved. However, the outlook is very promising because of the simplicity of the process and the nontoxicity of the carbon compounds involved, unlike cyanide-containing carbon compounds.

The principle of acid-base chromatography applied to the separation of carbon isotopes can also be applied to those materials for which conventional separation technologies are not effective. One successful application is chromatographic separation of rare-earth elements (*12*). This technology can also be applied to the separation of isotopes utilizing a reaction between solid and liquid phases which exhibits a clear isotope effect like that of bicarbonate.

CONCLUSIONS

1. The standard reduction potential strengths of ion-exchange and acid-base reactions were introduced and determined according to the definition.
2. The S potential of each carbonic species was calculated and

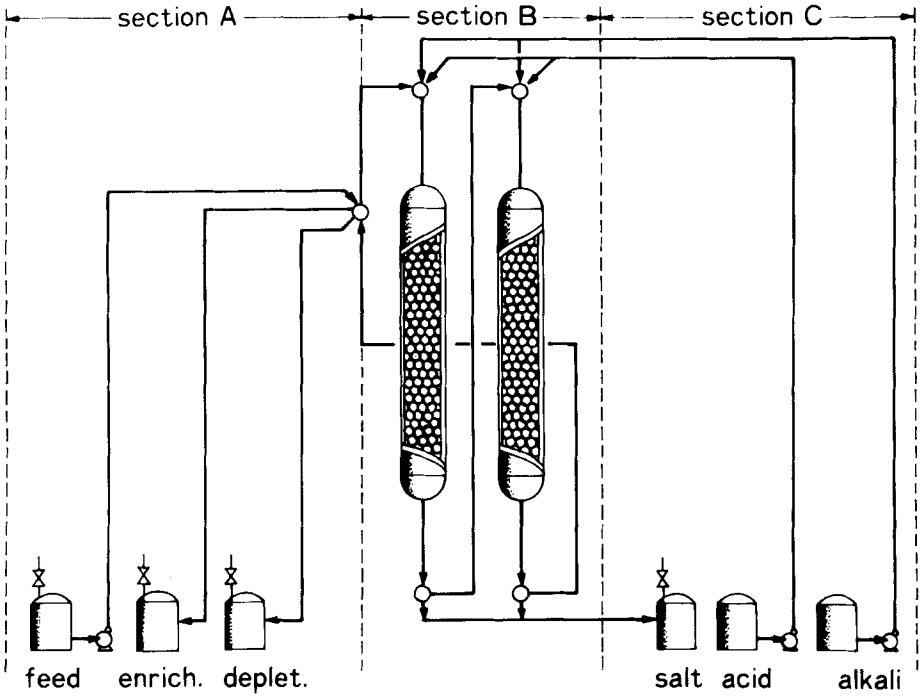

FIG. 7. Flow diagram of acid-base chromatography for carbon isotope separation. Section A is the feed and recovery section, Section B is the separation module, and Section C is the acid-base section.

conveniently used to determine its distribution by the function T_{i,n_j}.

3. The values of L potential sharply varied at both boundaries of the bicarbonate adsorption band, which resulted in forming the stable band and refluxing at both boundaries.
4. The separation factor observed in acid-base chromatography had the same value as that in solution.
5. Effective separation of ^{13}C was attained, and the ^{13}C-enriched solution could be recovered from the rear boundary of the bicarbonate band.

Acknowledgment

We are very grateful to Professor Manabu Seno of Tokyo University for his valuable suggestions and discussion.

REFERENCES

1. H. London, *Separation of Isotopes,* Newnes, London, 1961.
2. C. A. Hutchinson, D. W. Stewart, and H. C. Urey, *J. Chem. Phys., 8,* 532 (1940).
3. D. W. Stewart, *Nucleonics, 1,* 18 (1947).
4. H. C. Urey, A. H. W. Aten Jr., and A. S. Keston, *J. Chem. Phys., 4,* 622 (1936).
5. A. F. Reid and H. C. Urey, *Ibid., 11,* 403 (1943).
6. M. Seko, T. Miyake, K. Inada, and K. Takeda, *Nucl. Technol., 50,* 178 (1980).
7. M. Seko, T. Miyake, and K. Takeda, *Nippon Genshiryoku Gakkaishi, 20,* 547 (1978).
8. T. Miyake, K. Takeda, K. Imamura, and H. Obanawa, *Nucl. Technol., 64,* 237 (1984).
9. K. Takeda, F. Kawakami, and M. Sasaki, *Denki Kagaku Oyobi Kogyo Butsuri Kagaku, 53*(6), 385 (1985).
10. L. G. Sillen and A. E. Martell (compiled), *Stability Constants,* Chemical Society, London, 1964.
11. J. C. Giddings, *Dynamics of Chromatography: Part I; Principles and Theory,* Dekker, New York, 1965.
12. K. Takeda, M. Akiyama, F. Kawakami, and M. Sasaki, *Bull. Chem. Soc. Jpn., 59,* 2225 (1986).

Received by editor April 28, 1986